21ST INTERNATIONAL WORKSHOP ON RADIATION IMAGING DETECTORS
7–12 JULY 2019
CRETE, GREECE

Effects of p doping on GaAs/AlGaAs SAM-APDs for X-rays detection

C. Nichetti,[1,a,b] **T. Steinhartova,**[1,2b,c] **M. Antonelli,**[a] **G. Biasiol,**[c] **G. Cautero,**[a,d] **D. De Angelis,**[b] **A. Pilotto,**[f] **F. Driussi,**[f] **P. Palestri,**[f] **L. Selmi,**[g] **F. Arfelli,**[b,d] **M. Danailov**[a] **and R.H. Menk**[a,d,e]

[a] *Elettra-Sincrotrone Trieste S.C.p.A, Area Science Park Basovizza, 34149 Trieste, Italy.*
[b] *Department of Physics, University of Trieste, 34128 Trieste, Italy.*
[c] *IOM CNR, Laboratorio TASC, Area Science Park Basovizza, 34149 Trieste, Italy.*
[d] *Istituto Nazionale di Fisica Nucleare, INFN Sezione di Trieste, Trieste, 34100, Italy.*
[e] *Department of Medical Imaging, University of Saskatchewan, SK S7N 5A2, Canada.*
[f] *DPIA, University of Udine, Via delle Scienze 206, 33100 Udine, Italy.*
[g] *DIEF, University of Modena and Reggio Emilia, Via Trovarelli 2, 44100 Modena, Italy.*

E-mail: steinhartova@iom.cnr.it

ABSTRACT: This work focuses on avalanche photodiodes based on GaAs/AlGaAs with separated absorption and multiplication regions (SAM-APDs). The two regions are separated by a thin p-doped layer which, under the application of a reverse bias, is able to confine the potential drop only in the multiplication region. We realized such layer under the form of either a δ sheet of C atoms or a 50-nm-thick GaAs:C layer. Devices with these two structures will be discussed and compared in terms of capacitance and response to light.

KEYWORDS: Charge transport and multiplication in solid media; Detector design and construction technologies and materials; Solid state detectors; Voltage distributions

[1] These authors equally contributed to the work.
[2] Corresponding author.

Contents

1 Introduction

Fast, low noise X-ray detectors based on Avalanche PhotoDiodes (APDs) have the potential to pave the way to new and significant applications in scientific contexts such as synchrotron radiation facilities and free electron lasers. APDs have been traditionally based on silicon, as it is the most mature and robust technology. However, with the advent of latest generation light sources, more stringent requirements are put on detectors. In particular, in the energy ranges above 15 keV available in such sources the absorption of silicon drops considerably. To this aim, in GaAs-based semiconductors the higher Z number of Ga and As compared to that of Si leads to a much higher absorbance [9] and, accordingly, much thinner absorption regions are sufficient, resulting, in principle, in improved time resolution. However, a drawback of III-V materials is the similarity between electron and hole ionization coefficients, which increases the multiplication noise [2]. To compensate for this effect, band-gap engineered heterostructures have been proposed, which promote electron multiplication only [1]. In this respect, AlGaAs alloys can be synthesized in multilayers with varying composition within the device with state-of-the-art epitaxial techniques. We are developing APDs following such concept [1, 3, 11] including separated absorption and multiplication regions (SAM-APDs), see figure 1 c. The two regions are separated by a thin p-doped layer, with the aim of confining the potential drop mainly in the multiplication region under application of a reverse bias. In previous works [6], we have shown that acceptor sheet densities p of at least 2.5×10^{12} cm^{-2} are needed to obtain a complete electrostatic separation between the two regions. In this work, we have studied the behaviour of SAM APDs as p exceeds such threshold value. We found that up to 2.5×10^{12} cm^{-2}, p doping can be realized as a δ layer of C atoms (i.e., a 2D sheet of C atoms deposited during a growth interruption of the host GaAs material). However, since for higher C concentrations compensation effects take place [4], higher p dopings were obtained in 50-nm-thick GaAs:C layers. We have compared the capacitances under reverse bias of such devices and taken into account their response to visible light.

2 MBE growth and electrical characteristics

SAM APD samples were grown by Molecular Beam Epitaxy (MBE) following the protocols described in [6]. The p-doped layer separating the absorption and multiplication regions was

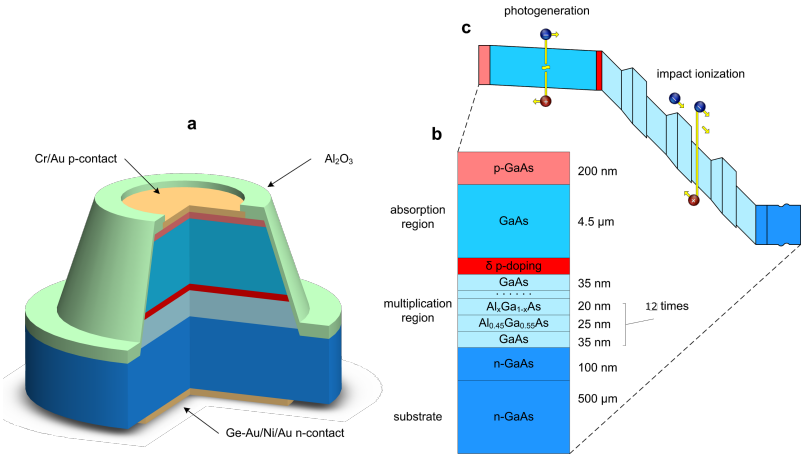

Figure 1. Schematics of the SAM-APD device structure (a), the layer sequence (b), and the band profiles under an applied bias (c). A 12× staircase GaAs/AlGaAs multilayer (multiplication region) is electrically separated from a 4.5 µm-thick GaAs absorption region by a p-doped layer, which ensures that, after applying a reverse bias, the vast majority of the potential drops in the multiplication region.

deposited under the form of either a δ sheet of C atoms or a 50-nm-thick GaAs:C layer. We calibrated the effective acceptor density in both cases by measuring the free carrier concentration at room temperature in a series of bulk GaAs samples containing either a δ or a 50-nm doped layer, with different planar densities of C atoms (figure 2), obtained by varying the current through the graphite filament of a carbon sublimation source. It was found that δ p-doped C layers are highly compensated, likely owing to atomic pairing [4]. Compensation takes places in the thin GaAs:C layers as well, although to a lesser extent. The maximum achievable acceptor densities were 2.5×10^{12} cm^{-2} and 1.2×10^{13} cm^{-2}, respectively. In the δ doping case, the dopant concentration p drops below its maximum by further increasing the source current.

Two SAM-APDs with the epitaxial structure of figure 1b and characterized by a mesa of 600 µm in diameter were grown by using either a δ carbon layer with $p = 2.5 \times 10^{12}$ cm^{-2} (device A) or a 50-nm GaAs:C with $p = 6 \times 10^{12}$ cm^{-2} (device B) to separate the absorption and multiplication regions.

The devices were fabricated as illustrated in figure 1a by the standard fabrication procedure described in [6], with the only difference that the passivation layer used was alumina (Al_2O_3).

In order to compare the shielding effect of the two doping distributions, the capacitance of devices A and B was measured as a function of the reverse bias, under dark conditions and at room temperature. These measurements were performed through a precision frequency LCR meter (HP4284A). The test signal was sinusoidal with a magnitude of 30 mV rms. These measurements were carried out at reverse voltages between 0 V and 35 V. The width of the depletion layer of the diodes as a function of the applied voltage was computed by using the measured capacitance as

$$d = \frac{\varepsilon_r \varepsilon_0 A}{C(V)} \tag{2.1}$$

where A is the area of the mesa, C is the measured capacitance, $\varepsilon_r = 12.6$ [7] and $\varepsilon_0 = 8.854 \cdot 10^{-12}$ F/m are the equivalent relative permittivity of the active region (calculated as the average

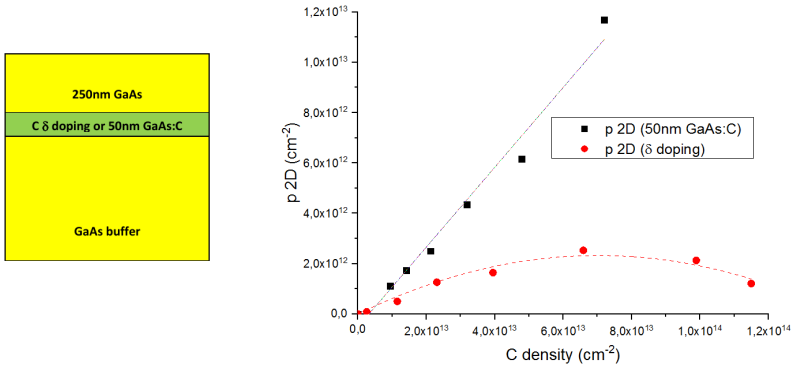

(a) (b)

Figure 2. (a) Schematics of the structures used for calibration of the p doping density; (b) acceptor density in the C-doped layers as a function of the 2D density of C atoms, showing that the effective 2D doping density is much lower than the 2D density of deposited C atoms. The dash lines are just to guide the eye.

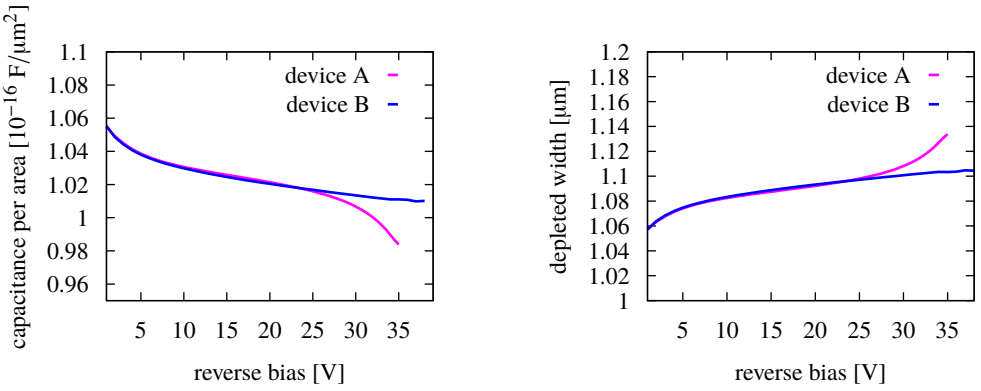

(a) (b)

Figure 3. (a) Experimental CV characteristics of devices with δ separation layer of acceptor density of 2.5×10^{12} cm^{-2} (A) and 50-nm separation layer of acceptor density of 6×10^{12} cm^{-2} (B); (b) their respective depletion width.

value of the permittivity of the different materials in the depletion region) and the permittivity of vacuum, respectively. Figure 3a shows the capacitance per area of the two photodiodes under comparison. The depleted width is in both cases close to 1 µm (figure 3b), which corresponds to the thickness of the multiplication region. This shows that for the whole voltage range considered both the δ and the 50-nm p layers are able to separate completely the two regions from an electrostatic point of view, confining the potential drop mainly into the multiplication region. It can be seen, however, that for device A the depletion region starts to leak weakly into the multiplication region too for the highest biases.

Looking closer into the shape of the CV curves we can calculate the profile of p-dopant concentration inside the device, $P(d)$, by using the equation for general nonuniform distributions [8, 10]

$$\frac{d(1/C_A^2)}{dV} = \frac{2}{q\varepsilon_r\varepsilon_0 P(d)} \tag{2.2}$$

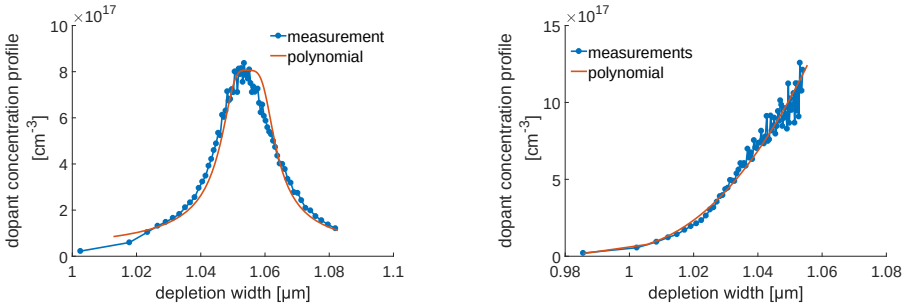

(a) (b)

Figure 4. Dopant concentration profile as a function of depletion width for devices A (a) and B (b). The blue dots represents the measured values, while the red continuous curve is the results of a polynomial fit of the inverse of the capacitance optimized with the least squares method, both obtained by using Equation 2.2. The fitting polynomials were introduced in order to obtain (after differentiation) noiseless reference curves which show the profiles also where the measured data become noisy.

where C_A is the capacitance per unit area of the mesa, V is the applied bias and q is the elementary charge and d is the depletion width, related to C_A through the data of figure 3. Since we are probing values of d in the proximity of the depletion width, we are sensitive to the charge distribution around the p-doped layer. From these analyses (figure 4) it follows that in the case of the 50-nm separation layer (B) the dopant concentration as a function of the distance below the junction between the p-layer and the intrinsic layer (which corresponds to the depletion region) grows monotonically. This trend testifies how the layer shields the absorption region in a way that the field has no measurable effect beyond the p-layer, at least within the voltages of operation. On the other hand, in the δ case the carrier concentration has a bell shape due to the drop in capacitance, which starts to occur in the devices with a just sufficient carbon concentration (A), meaning that in this case we start depleting beyond the δ-layer in the absorption region, as seen in figure 3b above.

3 Response to light

The devices were tested under a thermostated green tabletop laser (λ = 532 nm) to asses their response to light. Though they are suitable to be used under X-rays, the laser source was chosen in order to have ideal injection conditions (penetration depth = 140 nm [13]), meaning that electron and hole pairs are created just in a thin portion of the absorption region, not across the entire structure as when using higher photon energies. To compare the light responses of the devices we use the gain which is defined as

$$M = I_{\text{ph}}/I_{\text{pho}} \tag{3.1}$$

where I_{ph} is the difference between the measured photocurrent and the current measured under dark conditions and I_{pho} is I_{ph} when the multiplication does not occur [12]. The currents (figure 5a) were acquired through a 4-channel picoammeter (AH501 by Elettra). These data show that the absolute values of the photocurrent are higher in the case of device A even though the photon flux during acquisition was slightly lower (1400 vs. 1600 µ W). This could be explained by the fact that device A has a small residual field in the absorption region. This residual field makes

the created electrons drift towards the multiplication region, providing a better charge collection above 25 V. In absence of this field the charge carriers move just by diffusion resulting in a smaller charge collection efficiency and subsequently a smaller photocurrent even under higher photon flux ($\propto$1600 µW) in the case of the device B. The higher collection efficiency is also due to the different profile of the conduction band in the two cases, as it can be seen in figure 6. In fact, figure 6 shows that at higher concentrations (B) of the separation layer there is a larger initial step for the electrons to overcome with respect to the one obtained at lower concentrations (A). However, comparing the gains (figure 5b) of the devices A and B we can not see a significant difference in the behaviour. This is in agreement with the fact that the variation of the electric field intensity in the multiplication regions is relatively small compared to the already present one and it has no significant impact on the multiplication process.

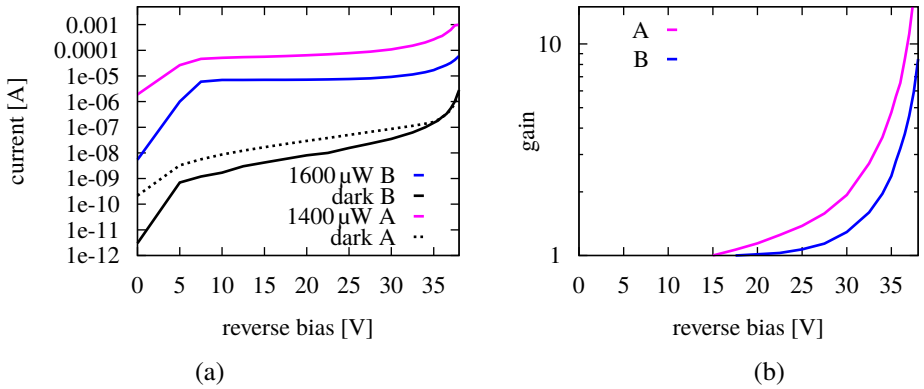

Figure 5. Currents (a) and gain (b) for device A (blue curve) and device B (magenta curve) as a function of the applied reverse bias. The power of the photon fluxes during the acquisition of the photocurrents for A and B were 1400 µW and 1600 µW, respectively.

4 Conclusions

We have studied the influence of the p-doped layer separating absorption and multiplication regions in GaAs/AlGaAs-based SAM APDs on their electrical characteristics and response to light. We have found that, in order to increase the doping above the minimum required to obtain sufficient electrostatic separation (2.5×10^{12} cm^{-2}), a thin (50 nm in our case) GaAs:C layer is needed, instead of the δ doping. Reverse-bias CV characteristics show that 2.5×10^{12} cm^{-2} doping is enough to confine the potential drop mainly in the multiplication r egion. However, a more detailed analysis reveals that, in contrast to higher doping, the depleted region extends slightly beyond the p layer for the highest applied biases, creating a residual field in the absorption r egion. This field seems to be beneficial for the collection efficiency of the devices as shown by comparing the absolute values of the photocurrent, while it does not influence significantly the multiplication pr ocess. Moreover, the higher concentration results in an obstacle for the electrons which are less likely to reach the multiplication region. In future, beside a further optimization of the dark characteristic, new devices with thicker absorption regions will be implemented and fabricated to be suitable under hard X-rays. Such thick layer could be obtained by MBE growth or using with advantage the intrinsic substrate as absorption region.

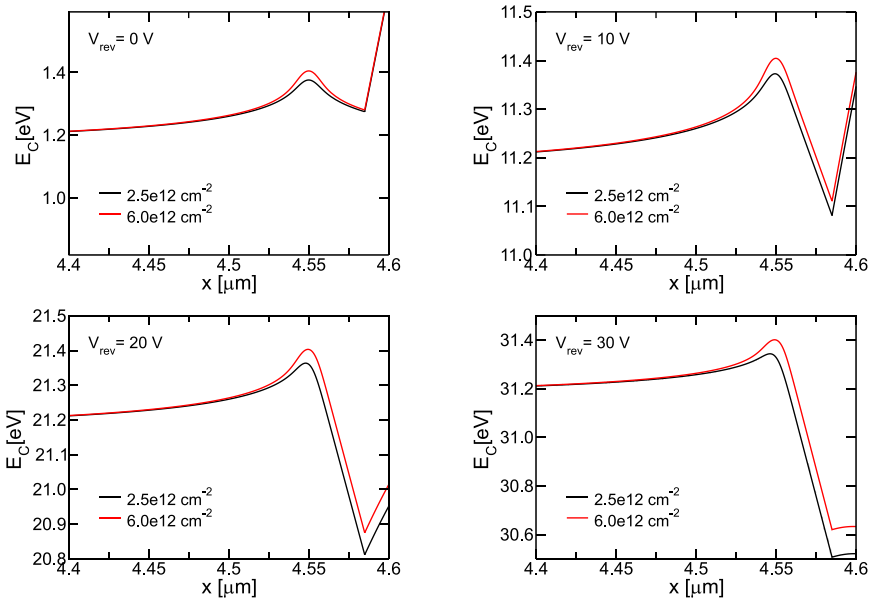

Figure 6. Conduction band profile, at different bias voltages, of the SAM-APD device structure in the surrounding of the layer dividing the absorption and the multiplication region. The red curve (device B) results always higher compared to the black one (device A), which means that the electrons encounter more difficulties in reaching the multiplication region in the first case compared to the latter one.

Acknowledgments

The research in this work received funding by the Italian MIUR through the PRIN 2015 project 2015WMZ5C8. Furthermore, the authors would like to thank A. Rachevski for his support during the experiments.

References

[1] F. Capasso, W.T. Tsang and G.F. Williams, *Staircase solid-state photomultipliers and avalanche photodiodes with enhanced ionization rates ratio*, *IEEE Trans. Electron Dev.* **30** (1983) 381.

[2] R.J. McIntyre, *Multiplication noise in uniform avalanche diodes*, *IEEE Trans. Electron Dev.* **ED-13** (1966) 164.

[3] J. Lauter, D. Protic, A. Forster and H. Luth, *AlGaAs/GaAs SAM-avalanche photodiode: an X-ray detector for low energy photons*, *Nucl. Instrum. Meth.* **A 356** (1995) 324.

[4] D.L. Sato, F.J. Szalkowski and H.P. Lee, *The theory of a general quantum system interacting with a linear dissipative Uniform and delta doping of carbon in GaAs by solid-source molecular beam epitaxy using electron beam evaporation: evidence for atomic pairing*, *Appl. Phys. Lett.* **66** (1995) 1791.

[5] *Synopsys, SentaurusTM Device User Guide*, (2016).

[6] T. Steinhartova et al., *Influence of p-doping on the behaviour of AlGaAs/GaAs SAM-APDs for synchrotron radiation*, 2017 *JINST* **12** C11017.

[7] M. Levinshtein and S. Rumyantsev, *Handbook series on semiconductor parameters. Volume 1*, World Scientific, Singapore (1996), see chapter 1.

[8] S.M. Sze, *Physics of semiconductor devices*, John Wiley & Sons, U.S.A. (1981).

[9] J.H. Hubbell, *Photon mass attenuation and energy-absorption coefficients from 1 keV to 20 MeV*, *J. Appl. Radiat. Isot.* **33** (1982) 1269.

[10] C. Nichetti et al., *Gain and noise in AlGaAs/GaA avalanche photodiodes with thin multiplication regions*, 2019 *JINST* **14** C01003.

[11] G.M. Williams, M. Compton, D.A. Ramirez, M.M. Hayat, A. and Huntington, *Multi-gain-stage InGaAs avalanche photodiode with enhanced gain and reduced excess noise*, *IEEE J. Electron Dev.* **1** (2013) 54.

[12] W.R. Clark et al., *Determination of quantum efficiency in $In_{0.53}Ga_{0.47}$ As-InP-Based APDs*, *J. Lightwave Technol.* **32** (2014) 4780.

[13] E.D. Palik, *Gallium Arsenide (GaAs)*, in *Handbook of optical constants of solids. Volume 1*, Academic Press, U.S.A. (1997).